

PCCP

Accepted Manuscript



This is an *Accepted Manuscript*, which has been through the Royal Society of Chemistry peer review process and has been accepted for publication.

Accepted Manuscripts are published online shortly after acceptance, before technical editing, formatting and proof reading. Using this free service, authors can make their results available to the community, in citable form, before we publish the edited article. We will replace this *Accepted Manuscript* with the edited and formatted *Advance Article* as soon as it is available.

You can find more information about *Accepted Manuscripts* in the [Information for Authors](#).

Please note that technical editing may introduce minor changes to the text and/or graphics, which may alter content. The journal's standard [Terms & Conditions](#) and the [Ethical guidelines](#) still apply. In no event shall the Royal Society of Chemistry be held responsible for any errors or omissions in this *Accepted Manuscript* or any consequences arising from the use of any information it contains.

***Ab initio* study of the thermoelectric enhancement potential
in nano-grained TiNiSn**

K. Kirievsky, M. Shlimovich, D. Fuks*, Y. Gelbstein

Materials Engineering Department, Ben Gurion University of the Negev,

Beer Sheva, Israel

*fuks@bgu.ac.il

Abstract

Novel approaches for development of highly efficient thermoelectric materials capable of a direct conversion of heat into electricity, are constantly investigated. TiNiSn based half Heusler alloys exhibit a high thermoelectric potential for practical renewable power generation applications. The main challenge on further enhancement of the thermoelectric efficiency of these alloys lies in the reduction of the associated high lattice thermal conductivity values without adversely affecting the electronic transport properties. The current manuscript, theoretically investigates two possible routes for overcoming on this limitation in TiNiSn alloys. On one hand, the influence of nano-grained structure of TiNiSn on the electronic structure of the material is theoretically demonstrated. On the other hand, the potential for thermal conductivity reduction with increasing the Ni fraction in the intermetallic TiNiSn compound, via the formation of metallic TiNi₂Sn nanoparticles is also shown. Using the applied approach, a useful route for optimizing both the electronic and thermal properties of half-Heusler TiNiSn, for practical thermoelectric applications, is demonstrated.

1. Introduction

In the last decade, the energy crisis had been a growing concern of the world community, due to overuse of fossil fuels and global warming. Significant efforts, applied all over the world aimed to solve the problem of affordable, environmentally clean energy. Thermoelectric energy based on a direct conversion of heat (or thermal gradient) into electricity is one possible solution for this complex problem. The efficiency of a thermoelectric material is proportional to the dimensionless figure of merit, ZT and the applied thermal gradient, highlighting the requirement of identifying highly efficient thermoelectric materials possessing large ZT values at any applications' operating temperatures. A number of new compounds have been investigated in the search for potential thermoelectric materials, including the half-Heusler alloys [1], capable of operation at

elevated ($>500^{\circ}\text{C}$) temperatures with adequate chemical, structural and mechanical stability. These materials are intermetallic alloys with the general formula MNiSn where M is a group IV transition metal (M=Zr, Hf, Ti).

The electronic structures and electrical transport properties of these alloys were previously studied using *ab initio* calculations and the Boltzmann transport equation under the constant relaxation time approximation for charge carriers [2]. Due to the simplicity of alloying of MNiSn (M=Ti, Zr, Hf) based compounds by substituting of their constituents by both iso-electronic and non-iso-electronic elements, new routes are constantly considered for optimizing their electronic and thermal properties. The papers by H. Hohl et al. [3] and by C. Uher et al. [4] were, seemingly, the first, demonstrating the beneficial effect of alloying on the M sublattice and of doping on the Sn site. Hf alloying on the Ti site and Sb doping on the Sn site lead to reduction of the lattice thermal conductivity and enhancement of the power factor, respectively. The results of optimization of the high temperature thermoelectric properties of TiNiSn by Hf alloying on the Ti site and Sb doping on the Sn site were reported, for example, in [5]. It was also established that changing the width of the band gap, controlling the number of charge carriers, increasing the slope of the density of states (DOS) for electrons in the vicinity of the bottom of conduction band, varying the scattering of electrons and phonons, etc. can be considered as promising methods for enhancement of the thermoelectric performance of related alloys. *Ab-initio* band structure calculations had been reported for analyzing the structural stability [6], the chemical bonding and the formation energies of antisite defects [7,8], as well as the elastic [9] and electronic properties [10-12] of Ni-containing MNiSn (M $\frac{1}{4}$ Ti, Zr, or Hf) compounds. Some efforts were directed to apply the concept of the valence electron content (VEC) and the calculated electronic band structure to expose factors that according to rigid-band considerations should determine the possible deviations from 1:1:1 stoichiometry and the direction of the stable solid-solution regions [13]. The results have been used to predict the direction of equilibrium solid-solution regions for a number of ternary phase diagrams that comprise half-Heusler phases. Fine features of the band structure of HH alloys are still under debates, but as discussed in [14] they are ultimately linked with the state of order in these compounds.

One of the current challenges is to reduce the relatively high thermal conductivity that is evident in these materials [15]. Two main methods being investigated trying to resolve the thermal conductivity issue and achieve higher power factor (the product of the square Seebeck coefficient and the electrical conductivity), are based on reduction of the average

grain size and electronically doping of the material, respectively. Most of the TiNiSn samples for experimental studies are prepared by the arc melting method and homogenized by various heat treatments, creating polycrystalline structures. The electronic properties of each sample are determined by the duration of the heat treatment and its temperature. Recent extensive investigation [16] of the microstructure in TiNiSn_{1-x}Sb_x series has established a significant decrease of the lattice thermal conductivity with the reduction of the average grain diameter, D , an effect which was found to be more pronounced for small (less than 10 μ m) grain size.

The aim of the current research is two-fold. On one hand, the influence of nano-grained structure of TiNiSn on the electronic structure of the material is theoretically demonstrated. On the other hand, the potential for thermal conductivity reduction with increasing the Ni fraction in the intermetallic TiNiSn compound, via the formation of metallic TiNi₂Sn nanoparticles is also shown. The first case was approached by comparative *ab initio* study of both TiNiSn monocrystal and nano-grained polycrystalline half-Heusler (HH) alloys. In the second case, the material's thermal conductivity variations based on calculated quasi-binary TiNiSn-TiNi₂Sn phase diagram, were estimated. The applied Density Functional Theory (DFT) calculations shed light on the nature of bonding in the interfaces between adjacent nano-grains for resolving the mechanisms affecting the electronic and thermal conductivity in the material. Using the applied approach, a useful route for controlling the thermal conductivity of HH TiNiSn by the introduction of embedded metallic TiNi₂Sn nano-inclusions, based on *ab initio* calculated thermodynamics phase diagram, is demonstrated.

2. Methodology

DFT using Full Potential method with Linearized Augmented Plane Waves (FP-LAPW) formalism, as implemented in the WIEN2k code (Version 10.1) [17-19] was applied in all of the calculations.

In this code the core states are treated as fully relativistic and the valence states are considered using a scalar relativistic approach. The exchange-correlation potential was calculated within the Perdew-Burke-Ernzerhof (PBE) generalized gradient approximation (GGA) [20]. The details of our calculations were as follows. The muffin-tin radii (R_{mt}) were taken equal to 1.9 Bohr for all of the atoms. For the basis-set size at each point, the cutoff parameter $R_{mt}K_{max} = 7$ was used where K_{max} presents the magnitude of the largest K vector in the wavefunction expansion. A maximal l , l_{max} , equal to 10 was taken in the expansion of the radial wave functions inside the atomic sphere to represent the valence states. The cut-off energy, separating core and valence states, was chosen as -6.0 Ryd for all of the atoms. This

condition is necessary in order to minimize the leak of the electron core states into the interstitial region. All of the integrations over the Brillouin zone (BZ) were performed using TEMPS scheme implied in WIEN2k with the broadening parameter in Fermi energy calculations equal to 0.002 that corresponds to $\sim 40^{\circ}\text{C}$. It was found that k-mesh of $8 \times 12 \times 8$ points, which corresponds to 216 k-points in the irreducible wedge of BZ, is sufficient to achieve $\sim 1 \cdot 10^{-3}$ Ryd accuracy in the total energy for all of cases applied in the self-consistent calculations.

For verification of the calculations' accuracy, the TiNiSn volume was optimized, as shown in Fig. 1. Several elastic, thermodynamic (see Table 1), and electronic properties (Fig. 2 and Table 2) of TiNiSn were calculated to justify the applicability of the FP-LAPW method. As can be definitely seen, the calculated results are in a good agreement with previously reported experimental and calculated data [22]. The currently calculated indirect Γ -X energy gap (0.45eV) is also in agreement with the previously reported 0.45eV [12, 23] and 0.468 eV [9] values.

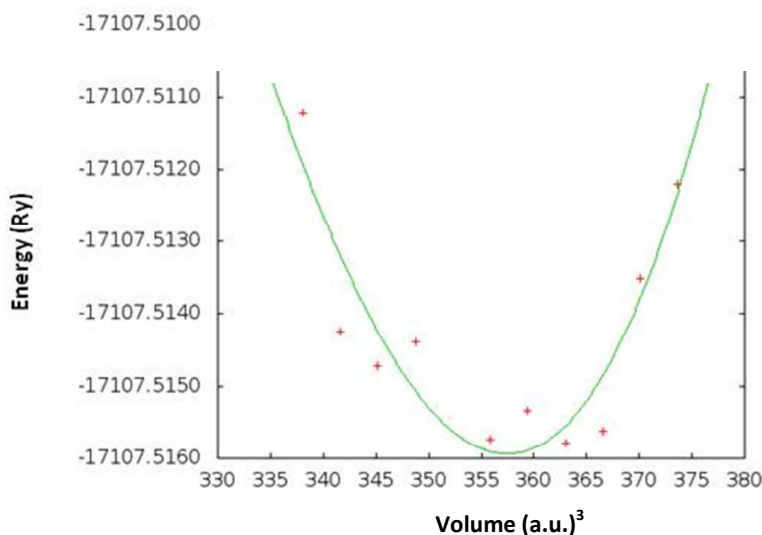


Fig. 1. Total energy vs volume optimization for TiNiSn. The fitting curve according to Murnaghan equation of states [21] is shown.

Table 1. Elastic and thermodynamic properties of TiNiSn

| Property | Current work | Experiment(*) and theory(**) |
|----------|--------------|------------------------------|
|----------|--------------|------------------------------|

| | | |
|---|--------|--------------------------|
| Cell parameter, a (Å) | 5.953 | 5.933* [22], 5.84** [24] |
| Bulk modulus, B (GPa) | 128 | 121** [25] |
| Shear modulus, G (GPa) | 75.52 | 87.84** [24] |
| Young modulus, E (GPa) | 189.28 | 219.96** [24] |
| Poisson ratio | 0.25 | 0.25** [24] |
| Debye temperature, Θ_D , (K) | 415 | 417* [26], 335* [27] |
| Enthalpy of formation, ΔE (kJ/mole) | -271.2 | -159** [25] |

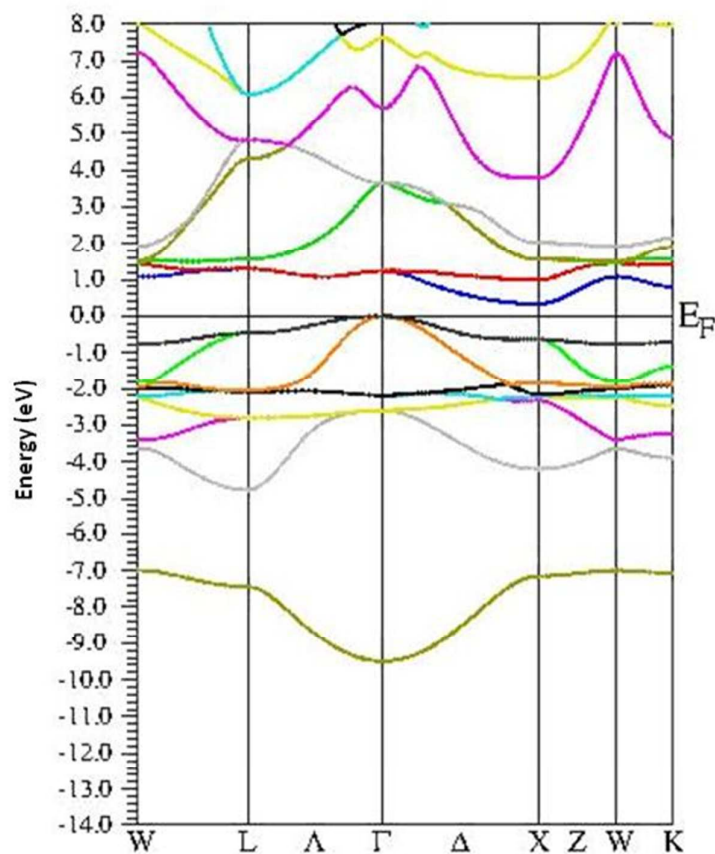


Fig. 2. Calculated energy bands for TiNiSn.

Table 2. Energy gaps in $E(k)$ for TiNiSn

| Property | Current work | Other works |
|--------------|--------------|-----------------------------------|
| E_g , [eV] | 0.45 | 0.42 [25], 0.47 [9], 0.45 [12] |

| | | |
|----------------------------|------|-----------------------------------|
| $E_{\Gamma \rightarrow L}$ | 1.45 | 1.41 [25], 1.49 [9], 1.42 [12] |
| $E_{\Gamma \rightarrow K}$ | 0.95 | 0.88 [25], 0.97 [9], 0.95 [12] |
| $E_{\Gamma \rightarrow W}$ | 1.15 | 1.17 [25], 1.27 [9], 1.15 [12] |

All of the currently performed Density of states calculations for TiNiSn were also found to be in a good agreement with those, reported in [25], where the DFT calculations were performed with the Vienna ab initio simulation package (VASP) [28] and with the projector augmented waves (PAW) technique [29,30].

Following the accuracy validation of the applied modeling approach, the comparative analysis of nano-grained TiNiSn was approached. In this study, $\Sigma 5$ 36.9°[100] tilt grain boundary (GB) in TiNiSn was considered between adjacent nano-grains of ~ 20 Å, each.

The supercell model for nano-grain boundary in the TiNiSn structure, shown in Fig. 3, was constructed using the GB Studio 3.0 software [31].

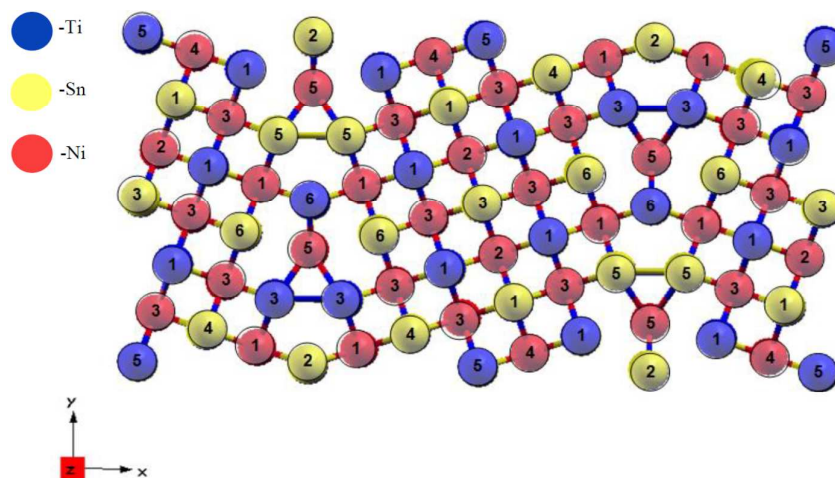


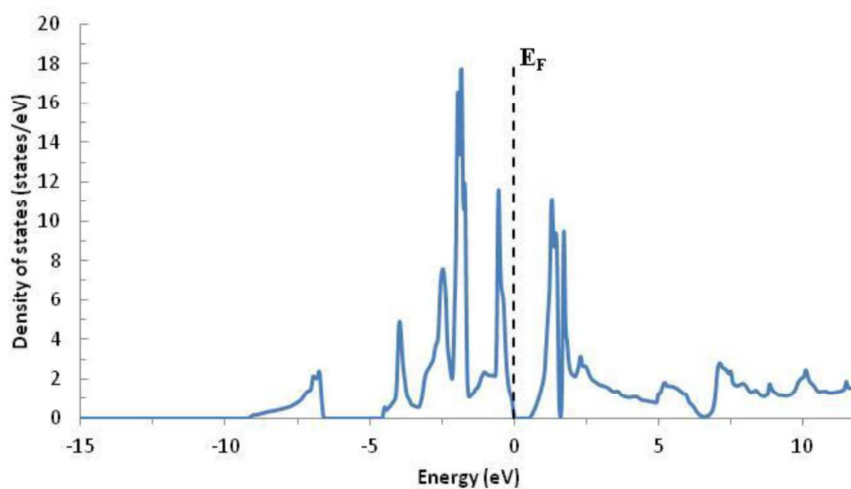
Fig. 3. Supercell top view, as was applied for modeling of the $\Sigma 5$ 36.9°[100] tilt grain boundary in TiNiSn.

3. Results and Discussion

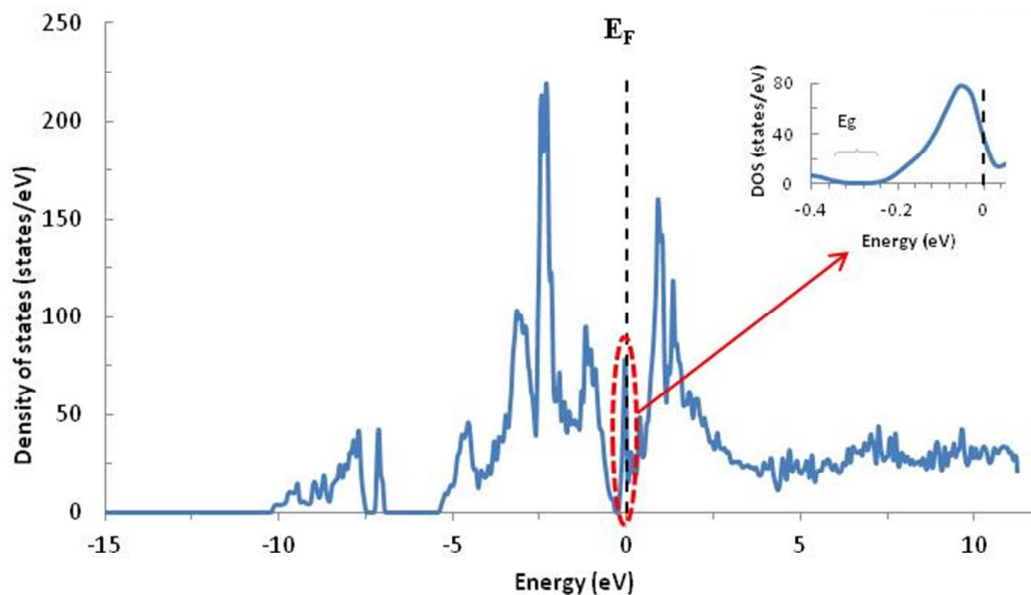
A) Nano-grained TiNiSn

The reduced supercell with 116 non-equivalent atoms was considered in the following analysis. The atoms positions in the vicinity of the GB were relaxed using the force minimization technique as implied in WIEN 2k code. The calculations were continued until the Hellman–Feynman forces became less than ~ 0.05 eV/Å. The calculation results indicated very small atoms displacements, with a decreasing order from the GB geometrical plane, toward the grain's interior. For example, for Ni atoms in the GB, the absolute value of the displacement does not exceed 3% of the lattice parameter. For all of the atoms, the displacements decrease exponentially and may be already neglected at the distanced third atomic layer from the GB. The calculated energy gain due to relaxation, was found to be $\sim 1.5 \cdot 10^{-2}$ Ry for the chosen supercell.

Total density of states (DOS) calculations for electrons are presented in Fig.4. While comparing the calculated results for mono-crystal and nano-grained TiNiSn, it may be seen that in the latter case, the energy gap, E_g becomes smaller, ~ 0.15 eV, and Fermi energy, E_F is shifted to the right. It crosses the additional states that appear due to the lattice broken symmetry and due to the interface formation between the grains.



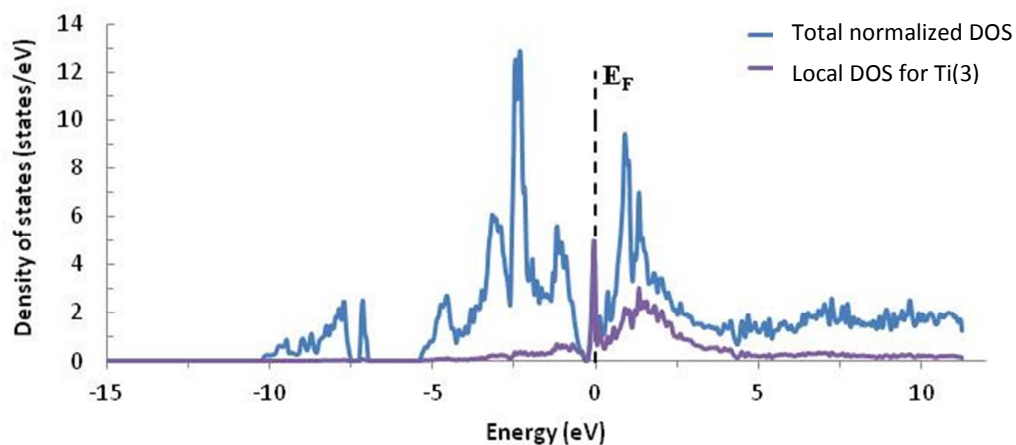
(a)



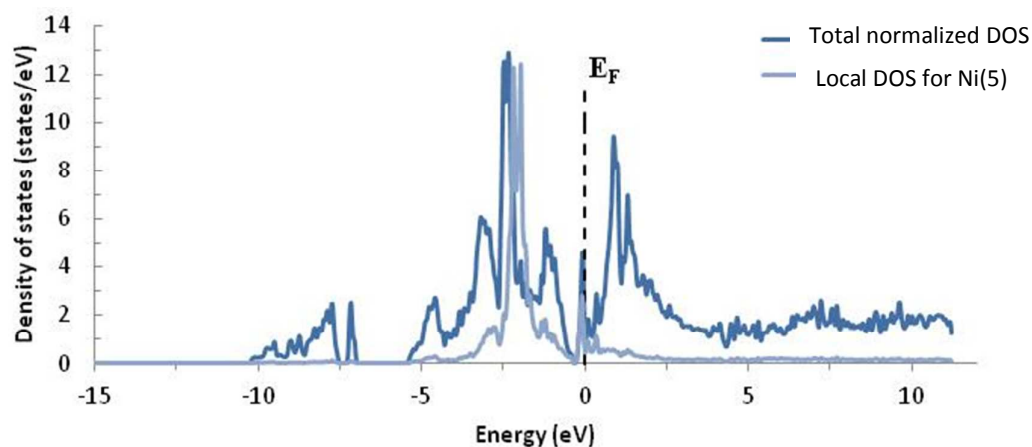
(b)

Fig. 4. Total DOS for mono-crystal (a) and nano-grained (b) TiNiSn. Dashed vertical line shows the position of Fermi energy, E_F . The inset illustrates an enlarged region in the vicinity of E_g .

The appeared occupied states, for the nano-grained sample, are situated close to the bottom of the conduction band and may be considered as the reason for the n -type conductivity in TiNiSn polycrystalline material. The contribution of the states of Ti(3) and Ni(5) atoms in the vicinity of the GB to the total DOS is shown in Fig. 5. The atoms numbers correspond to the illustrated locations shown in Fig.3. The calculation results reveal that the most pronounced contribution to the interfacial states is originated from the states of Ti and Ni atoms located in the vicinity of the GB. Electrons of Ti(6) atom contributes similarly to Ti(3) local DOS, while the electrons from the rest Ti and Ni atoms contribute much less to the total DOS. All of the Sn electrons in the vicinity of the GB contribute negligible input to the total DOS. Analysis of the partial DOS indicates that the main contribution to the local DOS originates from d -states of the corresponding Ti and Ni atoms.



(a)



(b)

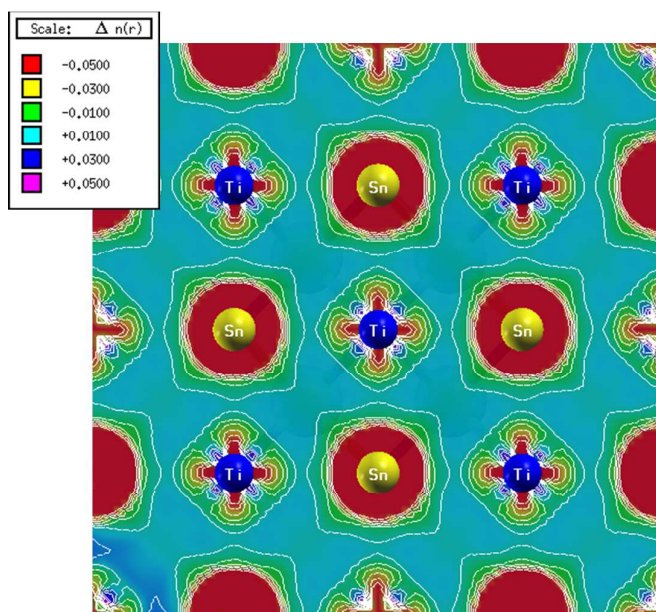
Fig. 5. Comparison of the total DOS normalized per atom in the investigated supercell with the local DOS for Ti and Ni in the vicinity of the GB. The total DOS for the supercell was normalized by dividing the density of states by the number of non-equivalent atoms in the supercell.

Additional information about the behavior of the charge carriers in the vicinity of the GB may be gained by electron density calculations in this region.

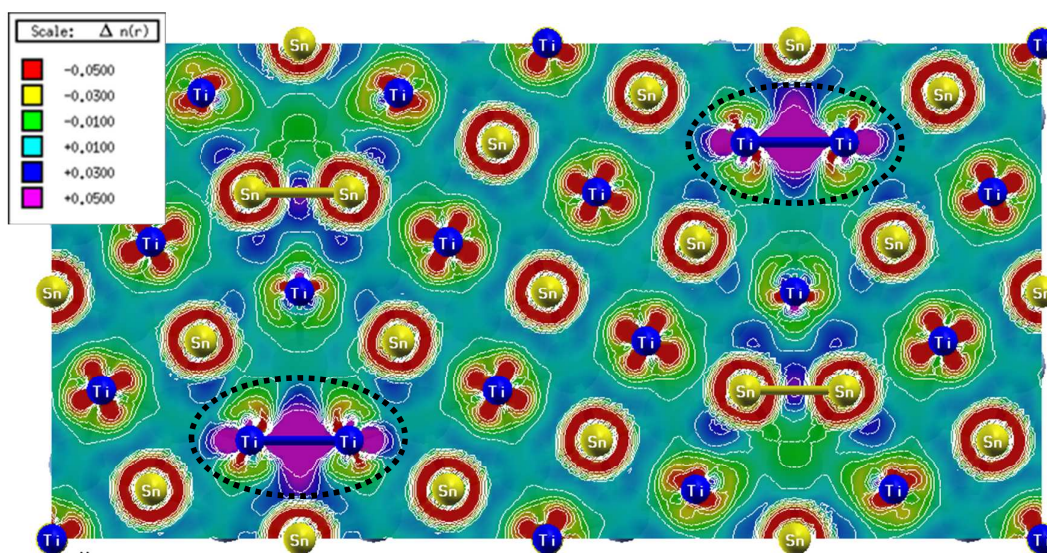
For this purpose, differential electron density maps were calculated for an ideal TiNiSn structure and for the polycrystalline material in the GB region, as can be shown in Fig. 6. This electron density is determined as the difference between the sum of the electron densities of the involved atoms and the electron density in the crystal structure obtained as the result of the density re-distribution, calculated in a self-consistent procedure.

Fig. 6a shows the regular symmetric electrons distribution in the monocrystal, while

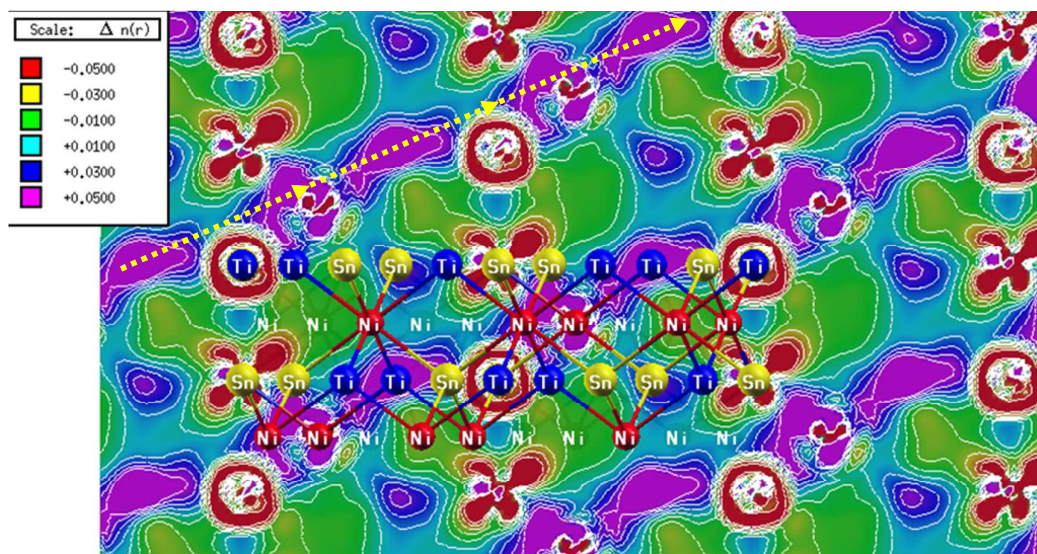
Figs. 6b,c clearly demonstrate the charge transfer in the vicinity of the GB. The cross section of the electron density in the (001) plane between adjacent grains (Fig.6b) is characterized by significant increase and delocalization of electrons of Ti(6) atoms in accordance with the formation of additional peaks in of the calculated DOS. In the GB plane, the charge delocalization is even higher, showing an increase of the fraction of the extra electrons in various directions. The yellow dotted arrows in Fig. 6c indicate the possible channel of additional charge transfer, stimulating the n-type conductivity of the nano-grained material.



(a)



(b)



(c)

Fig. 6. Cross-sections of the differential electron density distribution in TiNiSn: a) regular (0,0,1) plane in TiNiSn, b) (0,0,1) plane in the vicinity of GB in the polycrystalline TiNiSn, c) the GB plane. The scale is in electrons/Å³.

B) Nanoinclusions of TiNi₂Sn in TiNiSn

Creating full-Heusler nanoinclusions in the half-Heusler matrix was first put in practice in [32,33] based on the earlier study [34] who found that excess doping by Co or Ir on the Ni sublattice leads to an occupation of the previously empty sites on this sublattice.

Recently, DFT calculations were combined with statistical thermodynamics to construct the quasi-binary phase diagram of the TiNi_xSn system with $0 \leq x \leq 2$ [35]. It was demonstrated that in the $1 \leq x \leq 2$ atomic fraction range, for temperatures beyond $T=0\text{K}$, a decomposition into half-Heusler (HH) TiNiSn compound and $\text{TiNi}_{2-\delta}\text{Sn}$ Heusler alloy with the small deficiency, δ , on the Ni sub-lattice, occurs. This decomposition leads to the formation of nano-inclusions of Heusler phase embedded in the TiNiSn matrix, for x slightly larger than 1. Such decomposition was also experimentally verified (see for example, [36,37]). Formation of nano-inclusions in stoichiometric TiNiSn HH phase is considered as a promising approach for reduction of the thermal conductivity of thermoelectric materials [36,38-40]. The calculated phase diagram not only bridges the gap between the DFT calculations at $T=0\text{K}$ and the behavior of the system at elevated temperatures but also enables a better understanding of the expected thermal conductivity tendencies in the system for varied Ni atomic fractions and temperatures. Keeping in mind that the main thermal conductivity scattering mechanism is by short wavelength phonons in the inclusions and considering the calculated quasi-binary phase diagram (see Fig. 7), several *qualitative* conclusions may be formulated based on the lever rule for phase diagrams. For $\text{TiNi}_{1+y}\text{Sn}$ alloy with small y values, the diagram predicts the decomposition of the alloy into the primary TiNiSn compound and a small amount of $\text{TiNi}_{2-\delta}\text{Sn}$ secondary phase ($y=2x_0-1$). The secondary phase is expected to follow the morphology of nano-inclusions embedded in the TiNiSn matrix. At constant temperature, increasing the y value (for small y), leads to growth of the TiNi_2Sn phase fraction. Assuming that the shape and size of these separated TiNi_2Sn inclusions remain the same (which is reasonable for small deviations of y), the inclusions increased fraction will increase the scattering centers amount for short wavelength phonons and the thermal conductivity will decrease.

When the temperature increases at *constant* x_0 , $x_2 > x_1$ (see Fig. 7). Applying the lever rule will result in $\frac{x_0-0.5}{x_1-0.5} > \frac{x_0-0.5}{x_2-0.5}$, leading to increased fraction of the TiNi_2Sn nanoparticles and consequently to the reduction of the thermal conductivity. Both of the tendencies were observed experimentally [36].

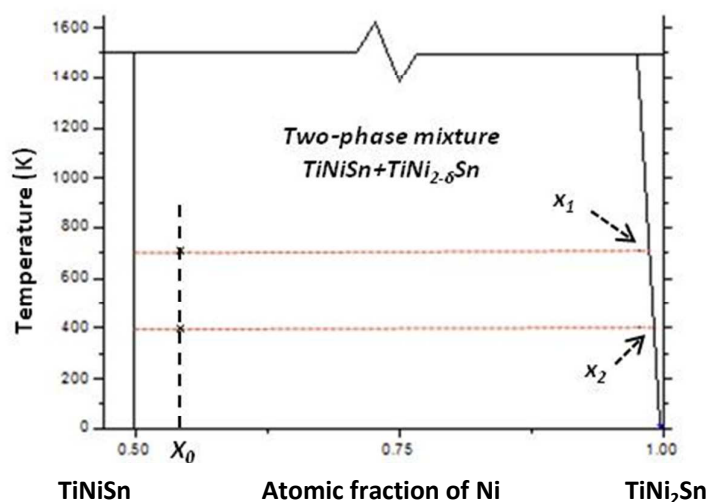


Fig. 7. Calculated quasi-binary TiNiSn-TiNi₂Sn phase diagram with the atomic fraction of Ni on the simple cubic sub-lattice sites immersed in the field of the NaCl-type sub-lattice of TiSn background.

Additional *quantitative* information that allows an estimation of the influence of the Ni content on the thermal conductivity might be obtained from the calculated phase diagram, based on the thermoelectric formulation derived recently for embedded metallic nano-inclusions inside a semiconducting matrix [41]. As can be seen from the calculated DOS for TiNi₂Sn (see Fig. 8), this phase is metallic without an energy gap in the vicinity of E_F .

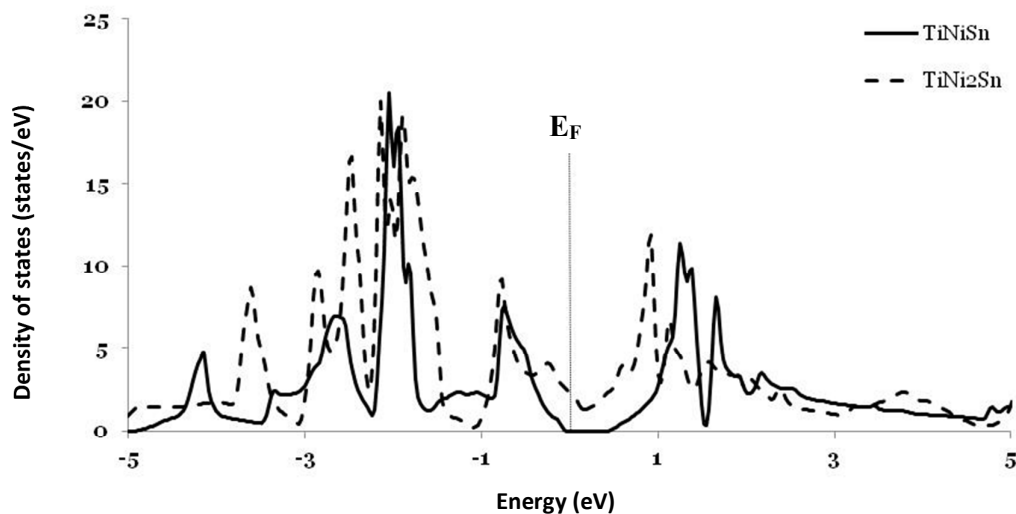


Fig. 8. Comparison of the DOS for TiNiSn and TiNi₂Sn.

As follows from the calculated phase diagram, for small x_0 , the Ti-Ni-Sn system decomposes, and its morphology is characterized as a two-phase mixture of small well-separated nanoparticles of metallic TiNi_2Sn embedded in a TiNiSn semiconductor. It was demonstrated in [41] that for weakly-doped semiconductors, ZT enhancement might be primarily related to a decrease in the phonon thermal conductivity, K_{th} , expressed in eq. 1.

$$K_{th} = \frac{1}{3}C \langle v_s \rangle l = \frac{1}{3}C \langle v_s \rangle^2 \tau, \quad (1)$$

where $\langle l \rangle$ is a mean free path for phonons, C - heat capacity of the matrix per unit volume, $\langle v_s \rangle$ - average sound velocity, and τ - relaxation time, which in the current case can be described according to eq. 2.

$$\frac{1}{\tau} = \frac{1}{\tau_{matrix}} + \frac{1}{\tau_{inclusions}} \quad (2)$$

Our DFT calculated sound velocity, v_s , value for TiNiSn was found as 3630m/sec, while the corresponding v_s' value in TiNi_2Sn is 7511m/sec. Taking into account, the thermal conductivity for TiNiSn , $K_{th}=6\text{W}/(\text{m}\cdot\text{K})$ reported in [42] and the heat capacity from [43], τ_{matrix} is found to be $1.76\cdot 10^{-12}\text{sec}$. For $\tau_{inclusions}$, the expression derived in Refs. [44,45] in the near-geometrical scattering regime $qR \geq 1$ $\tau_{inclusions}$, presented in eq. 3, was employed.

$$\frac{1}{\tau_{inclusions}} = n_i v_s (2\pi R^2) \left[1 - \frac{\sin(2\gamma)}{\gamma} + \frac{\sin^2(\gamma)}{\gamma^2} \right], \quad (3)$$

where n_i is the inclusions concentration, $n_i = 3x/(4\pi R)^3$, x is the volume fraction of the TiNi_2Sn phase in the two-phase mixture, R is the inclusions radius, $\gamma = qR(v_s/v_s' - 1)$, and q is the phonon wave vector. For Ti-Ni-Sn with the above velocities, eq. 4, can be derived

$$\frac{1}{\tau_{inclusions}} = n_i v_s (2\pi R^2) = \frac{3x}{2R} v_s \quad (4)$$

with an accuracy of $\sim 3\%$. With $x \approx 0.048$ for $T=400\text{K}$ from the calculated phase diagram, corresponding to the experimental data for $\text{TiNi}_{1+y}\text{Sn}$ for $y=0.05$ from [36] and average TiNi_2Sn nano-inclusions radius, $R \sim 1\text{nm}$, $\tau_{inclusions} = 1.28 \cdot 10^{-12}\text{sec}$ was obtained. Substitution of the obtained τ_{matrix} and $\tau_{inclusions}$ in Eqs (2) and (1) gives $K_{th} = 4.34\text{W}/(\text{m}\cdot\text{K})$ that corresponds well with the experimental $K_{th} = 4.5 \pm 0.4 \text{ W}/(\text{m}\cdot\text{K})$ data reported by [36].

4. Conclusions

The influence of the nano-grained structure on the electronic properties and the thermal conductivity of TiNiSn based alloys was investigated in detail. The major findings of this investigation are summarized as follows:

1. Interfacial states formed in nano-grained TiNiSn play important role determining the n -type conductivity of the material. The changes in the atoms bonding in the vicinity of the grain boundaries (GB) lead to strong delocalization of the covalent bonds and stimulate the electron transport along the interfaces between the grains.

2. The formation of dense TiNi₂Sn nano-precipitates with small deficiency of Ni within the HH TiNiSn matrix might be explained in terms of decomposition as was revealed by the calculated phase diagram. This occurs when HH alloys are slightly enriched by Ni.

3. It is demonstrated that the calculated phase diagram might serve as a useful tool for thermal conductivity prediction in two-phase HH TiNiSn and TiNi₂Sn Heusler mixtures at different temperatures, for slightly higher Ni concentrations than the stoichiometric for TiNiSn. This finding might be useful in development of thermoelectric devices that are aimed to operate at different temperature regimes.

Formation of interfacial states in nano-grained narrow band gap TiNiSn enables new opportunities in engineering of novel beyond the state of the art thermoelectric materials, for example by grains size modifications while applying the powder metallurgy technique for synthesis of such materials.

Engineering of Heusler alloys following a decomposition into TiNi₂Sn nanoinclusions embedded within the TiNiSn semiconducting phase, was shown to be a promising route of controlling the materials' thermal conductivity and thereby improving the thermoelectric properties. Controlling the nanoprecipitates size and/or distribution by appropriate thermal treatment, according to the calculated relevant phase diagram, combined with a more complete morphological characterization might also be considered for thermoelectric optimization of such alloys.

Acknowledgement.

The work was supported by the Israel Science Foundation (ISF), Grant Nos. 497/12 and 1578/12. D.F. holds Stephen and Edith Berger Chair in Physical Metallurgy.

References

1. N. Shutoh and S. Sakurada, *J. of Alloys and Comp.*, 2005, **389**, 204–208.
2. J. Yang, H. Li, T. Wu, W. Zhang, L. Chen and J. Yang, *Adv. Funct. Mater.*, 2008, **18**, 2880-2888.
3. H. Hohl, A. P. Ramirez, W. Kaefer, K. Fess, Ch. Thurner, Ch. Kloc and E. Bucher, A new class of materials with promising thermoelectric properties: MNiSn (M=Ti,

- Zr, Hf), in *Thermoelectric materials – new directions and approaches*, eds. T. M. Tritt, M. G. Kanatzidis, H. B. Lyon, Jr. and G. D. Mahan, Materials Research Society, Pittsburg, Pa, *Mater. Res. Soc. Symp. Proc.*, 1997, **478**, pp. 109-114.
4. C. Uher, S. Hu and J. Yang, *Proc. 16th Int. Conf. on Thermoelectrics*, Piscataway, IEEE Catalog Number 97TH8271, 1997, pp. 485-488.
 5. S.-W. Kim, Y. Kimura and Y. Mishima, *Intermetallics*, 2007, **15**, 349-356.
 6. S. Ögut and K.M. Rabe, *Phys. Rev. B*, 1995, **51**, 10443-10453.
 7. P. Larson, S. D. Mahanti and M. G. Kanatzidis, *Phys. Rev. B*, 2000, **62**, 12754-12762.
 8. P. Qiu, J. Yang, X. Huang, X. Chen, and L. Chen, *Appl. Phys. Lett.* 2010, **96**, 152105-1-3.
 9. M. Hichour, D.Rached, R.Khenata, M.Rabah, M.Merabet, A. H. Reshak, S. BinOmran and R.Ahmed, *J. Phys. Chem. Solids*, 2012, **73**, 975-981.
 10. S. Kaprzyk and A. Bansil, *Phys.Rev. B*, 1990, **42** 7358-7362.
 11. A. Bansil, S. Kaprzyk, P. E. Mijnaerends and J. Tobola, *Phys.Rev. B*, 1999, **60**, 13396-13412.
 12. L. Chaput, J.Tobola, P.Pécheur and H.Scherrer, *Phys.Rev. B*, 2006, **73**, 045121-7.
 13. L. Offernes, P. Ravindran, C.W. Seim and A. Kjekshus, *J. of Alloys and Compounds*, 2008, **458**, 47-60.
 14. V.A. Romaka, P. Rogl, V.V. Romaka, E.K. Hlil, Yu.V. Stadnyk and S.M. Budgerak, *Semiconductors*, 2011, **45**, 850-856.
 15. S. Bhattacharya, A. L. Pope, R. T. Littleton, Terry M. Tritt, V. Ponnambalam and Y. Xia, *Appl. Phys. Lett.*, 2000, **77**, 2476-2478.
 16. S. Bhattacharya, M. J. Skove, M. Russell, T. M. Tritt, Y. Xia, V. Ponnambalam, S. Poon and N. Thadhani, *Physical Review B*, 2008, **77**, 184203-8.
 17. K. Schwarz, P. Blaha and G.K.H. Madsen, *Comput. Phys. Comm.*, 2002, **147**, 71-76.
 18. S. Cottenier, *Density Functional Theory and the Family of (L)APW Methods: A Step-by-Step Introduction*, Belgium 2002, ISBN 90-807215-1-4 (http://www.wien2k.at/reg_user/textbooks).
 19. P. Blaha, K. Schwarz, G.K.H. Madsen, D. Kvasnicka and J. Luitz, *WIEN2k, An Augmented Plane Wave + Local Orbitals Program for Calculating Crystal Properties* (Karlheinz Schwarz, Techn. Universitat Wien, Austria), 2001. ISBN 3-9501031-1-2, version 10.1 (release 10/6/2010).
 20. J.P. Perdew, K. Burke and M. Ernzerhof, *Phys. Rev. Lett.*, 1996, **77**, 3865-.

21. F. D. Murnaghan, The Compressibility of Media under Extreme Pressures, in *Proceedings of the National Academy of Sciences of the United States of America*, 1944, **30**, 244–247.
22. V.V. Romaka, P. Rogl, L. Romaka, Yu. Stadnyk, N. Melnychenko, A. Grytsiv, M. Falmbigl and N. Skryabina, *J. Solid State Chem.*, 2013, **197**, 103-112.
23. S. Ouardi, G.H. Fecher, B. Balke, X. Kozina, G. Stryganyuk, C. Felser, S. Lowitzer, D. Ködderitzsch, H. Ebert and E. Ikenaga, *Phys. Rev. B*, 2010, **82**, 085108-9..
24. M. Hichouretal, *J. Phys. Chem. Sol.*, 2012, **73**, 975–981.
25. C. Colinet, Ph. Jund and J.-C. Tédénac, *Intermetallics*, 2014, **46**, 103-118.
26. R. Kuentzler, R. Clad, G. Schmerber and Y. Dossmann, *J. Magn. Magn. Mater.*, 1992, **104-107**, 1976-8.
27. B. Zhong, *Physical metallurgy and properties of TiNiSn and PtMnSb*, M.Sc. Thesis, Iowa State University, 1997, p.50.
28. G. Kresse and J. Furthmüller, *Comp. Mater. Sci.*, 1996, **6**,15-50; *Phys Rev B*, 1996, **54**, 11169-11186.
29. P. E. Blöchl, *Phys Rev B*, 1994, **50**, 17953-17979.
30. G. Kresse, and D. Joubert, *Phys Rev B*, 1999, **59**,1758-1775.
31. H. Ogawa, *Mater. Transact.*, 2006, **47**, 2706- 2710.
32. J. P. A. Makongo, D. K. Misra, J. R. Salvador, N. J. Takas , G. Wangc, M. R. Shabetai, A. Pant, P. Paudel, C. Uher, K. L. Stokes and P. F. P. Poudeu, *J. Sol. State Chem.*, 2011, **184**, 2948-2960.
33. J. P. A. Makongo, D. K. Misra, X. Zhou, A. Pant, M. R. Shabetai, X. Su, C. Uher, K. L. Stokes and P. F. P. Poudeu, *J. Am. Chem. Soc.*, 2011, **133**, 18843-18852.
34. Y. Kimura, T. Tanoguchi and T. Kita, *Acta Mater.*, 2010, **58**, 4354-4361.
35. K. Kirievsky, Y. Gelbstein and D. Fuks, *J. Sol. State Chem.*, 2013, **203**, 247–254.
36. R. A. Downie, D. A. MacLaren, R. I. Smith and J. W. G. Bos, *Chem. Commun.*, 2013, **49**, 4184-4186.
37. Y. W. Chai and Y. Kimura, *Acta Mater.*, 2013, **61**, 6684–6697.
38. C. J. Vineis, A. Shakouri, A. Majumdar and M. G. Kanatzidis, *Adv. Mater.*, 2010, **22**, 3970–3980.
39. J. E. Douglas, C. S. Birkel, M.-S. Miao, C. J. Torbet, G. D. Stucky, T. M. Pollock and R. Seshadri, *Appl. Phys. Lett.*, 2012, **101**, 183902-4.
40. C. S. Birkel, J. E. Douglas, B. R. Lettiere, G. Seward, N. Verma, Y. Zhang, T. M. Pollock, R. Seshadriab and G. D. Stucky, *Phys. Chem. Chem. Phys.*, 2013, **15**,

- 6990-6997.
41. S. V. Faleev and F. Léonard, *Phys. Rev. B*, 2008, **77**, 214304-1-9.
 42. S. W. Kim, Y. Kimura and Y. Mishima, *Intermetallics*, 2007, **15**, 349-356.
 43. D. Wee, B. Kozinsky, B. Pavan and M. Fornari, *J. Electron. Mater.*, 2012, **41**, 977-983.
 44. W. Kim, J. Zide, A. Gossard, D. Klenov, S. Stemmer, A. Shakouri and A. Majumdar, *Phys. Rev. Lett.*, 2006, **96**, 045901-4.
 45. W. Kim and A. Majumdar, *J. Appl. Phys.*, 2006, **99**, 084306-7.